

Measurement of the mixed mode fracture strength of green sandstone using three-point bending specimens

Yifan Li^{*1,2}, Shiming Dong² and Martyn J. Pavier¹

¹Department of Mechanical Engineering, University of Bristol, Queens Building, University Walk, Bristol BS8 1TR, U.K.

²College of Architecture and Environment, Sichuan University, Chengdu 610065, China

(Received August 29, 2019, Revised December 7, 2019, Accepted December 23, 2019)

Abstract. Three-point bending specimens have been used to investigate the mixed mode fracture of green sandstone. Dimensionless stress intensity factors and T-stresses were calculated first by using the finite element method for various crack lengths, crack angles and span to length ratios. It is shown that three-point bending specimens can provide the whole range of mode mixities from pure mode I to pure mode II, provided suitable values are chosen for the crack angle and span to length ratio. The fracture test results were also used to compare with predictions of different criteria. These comparisons show that modified criteria including the influence of the T-stress agree better with experiment than the conventional criteria but that no one criterion matches perfectly the test results.

Keywords: sandstone; fracture; T-stress; three-point bending; different criteria

1. Introduction

Brittle fracture is the most common form of failure in rock structures. Because a crack in a rock mass has an arbitrary direction relative to the applied load, most rock fractures occur under mixed mode conditions (Aliha and Ayatollahi 2011). Numerous criteria have been developed to predict mixed mode fracture including the maximum tangential stress (MTS) criterion, minimum strain energy density (SED) criterion, and the maximum tangential strain (MTSN) criterion (Erdogan and Sih 1963, Sih 1973, Sih 1974, Chang 1981). In this paper, these criteria ignoring the influence of T-stress will be referred collectively to as conventional criteria.

In recent years, researchers have found that the T-stress, has a significant effect on the fracture behavior of rock. In many practical cases, a large discrepancy has been reported between predications of rock fracture using conventional mixed mode criteria and experimental results. Smith *et al.* (2001) proposed a generalized maximum tangential stress (GMTS) criterion based on the MTS criterion, which includes the effect of T-stress. Different types of rock material have been studied by Ayatollahi *et al.* (2008, 2011) and Aliha *et al.* (2010), and they found that the GMTS criterion matches experimental results better than the MTS criterion, including the fracture resistance and crack initiation angle. More recently, a generalized minimum strain energy density (GSED) criterion and generalized maximum tangential strain (GMTSN) criterion have been proposed by different researchers (Ayatollahi and Sedighiani 2012, Ayatollahi *et al.* 2015, Mirsayar 2015, Hua

et al. 2017), which generally show better results for rock materials than other criteria. The generalized maximum tangential strain (GMTSN) criterion has been used using different brittle materials such as rock and graphite, showing that the criterion provides improved predictions (Mirsayar *et al.* 2016, Mirsayar *et al.* 2018). Another modified SED criterion called the average strain energy density (ASED) criterion was mentioned and mainly used in specimens with sharp V-notches, and the predicting results, like the fracture load, are in good agreement with the experimental results (Ayatollahi *et al.* 2017, Campagnolo and Berto 2017, Razavi *et al.* 2018). These criteria will be referred to here as modified criteria. Most existing work on rock fracture has not used the range of mixed mode criteria to compare with test results, although Aliha *et al.* (2013) used compared the results of fracture tests on Neiriz marble with the GMTS, MTS and SED criteria.

The third terms of the Williams expansion, usually denoted as A_3 and B_3 , also have a significant effect on the fracture behaviour of rock and other geo-materials. Aliha *et al.* (2012) analysed statistically the A_3 effects on mode I fracture resistance ($K_{I\text{ff}}$) by two different test samples and found that negative A_3 increases the mode I fracture resistance while positive A_3 decreases it. Akbaridoost and Ayatollahi (2014) proposed the modified MTS criterion (MMTS) taking into account not only the SIF and T-stress but also these third terms. They compared the predictions with experimental results using a circular disk specimen and an edge-cracked triangular specimen. Ayatollahi and Akbaridoost (2012, 2013) also studied size effects for mode I and mode II fracture toughness of geo-materials by using a stress-based criterion including the third terms.

Different methods and specimen types have been used to study the fracture properties of rock materials. Disc-shaped specimens such as the central cracked Brazilian disk (CCBD) and edge cracked semi-circular (SCB) specimens

*Corresponding author, Ph.D. Student
E-mail: yifan.li@bristol.ac.uk

have been widely used (Aliha *et al.* 2010, Maruvanchery and Kim 2019), because the test configurations are straightforward and are suitable for a wide range of mode mixities. Another disc-shaped specimen called the edge-notched disc bend specimen (ENDB) proposed by Aliha *et al.* (2015a) can introduce complete mode I/III mixities including pure mode I and pure mode III fracture by rotating the crack plane. Numerous studies have shown that this specimen can be utilized successfully to study mixed mode I/III fracture behaviour of engineering materials like rock, graphite, PMMA, and asphalt (Aliha *et al.* 2015b, Aliha and Bahmani 2017, Pour *et al.* 2018). However, disc type specimens are generally more difficult to prepare (Aliha *et al.* 2013). Other test methods such as the compact tension–shear specimen and angled internal cracked plate require complicated fixtures and loading setup (Richard and Benitz 1983, Yukio *et al.* 1983). Three-point bending specimens are frequently used because of the easy processing procedure and simple loading conditions. It can also be easily cut from rock masses at any desired size. However, three-point bending specimens are mainly used to study the pure mode I fracture and I/II mixed mode fracture properties of materials (Midhun *et al.* 2018, Kumar *et al.* 2017, Rizov 2013). Few researchers have used three-point bending specimens to do pure mode II fracture tests although recently, Aliha *et al.* (2018, 2019) investigated the fracture toughness of bovine bone and bitumen under different mode mixities using a compact beam bend specimen and showed that the specimen can produce full combinations of mode mixities from pure mode I to pure mode II. Other studies have shown that this specimen is able successfully to produce and characterize mixed mode I/II fracture behavior of brittle materials such as PMMA (Mousavi *et al.* 2019, Shaker *et al.* 2019).

In this paper, several criteria that include the effect of T-stress will be reviewed. A finite element study has been used to demonstrate that a three-point bending specimen can provide the full range of mode mixities, from pure mode I to pure mode II. A series of mixed mode three-point bending fracture tests have been conducted, and the results compared with predictions obtained using a range of criteria.

2. A brief introduction to fracture criteria

The stress field for a linear elastic material around the crack tip under general mixed mode I/II conditions (Fig. 1), which considers both the singular terms and the T-stress could be expressed in the form of a series expansion with Williams's infinite terms (Williams 1957):

$$\begin{aligned}\sigma_{rr} &= \frac{1}{\sqrt{2\pi r}} \left[K_I \left(\frac{5}{4} \cos \frac{\theta}{2} - \frac{1}{4} \cos \frac{3\theta}{2} \right) + K_{II} \left(-\frac{5}{4} \sin \frac{\theta}{2} + \frac{3}{4} \sin \frac{3\theta}{2} \right) \right] + T \cos^2 \theta + O(r^{\frac{1}{2}}) \\ \sigma_{\theta\theta} &= \frac{1}{\sqrt{2\pi r}} \left[K_I \left(\frac{3}{4} \cos \frac{\theta}{2} + \frac{1}{4} \cos \frac{3\theta}{2} \right) + K_{II} \left(-\frac{3}{4} \sin \frac{\theta}{2} - \frac{3}{4} \sin \frac{3\theta}{2} \right) \right] + T \sin^2 \theta + O(r^{\frac{1}{2}}) \\ \tau_{r\theta} &= \frac{1}{\sqrt{2\pi r}} \left[K_I \left(\frac{1}{4} \sin \frac{\theta}{2} + \frac{1}{4} \sin \frac{3\theta}{2} \right) + K_{II} \left(\frac{1}{4} \cos \frac{\theta}{2} + \frac{3}{4} \cos \frac{3\theta}{2} \right) \right] - T \sin \theta \cos \theta + O(r^{\frac{1}{2}})\end{aligned}\quad (1)$$

where K_I and K_{II} are the mode I and mode II stress intensity factors and T is the T-stress. The higher order terms $O(r^{1/2})$ can be considered negligible near the crack tip.

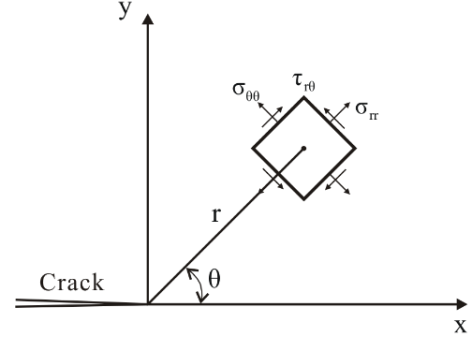


Fig. 1 The stress components around the crack tip

The effective stress intensity factor K_{eff} is often used in mixed mode fracture criteria. It is written as

$$K_{eff} = \sqrt{K_I^2 + K_{II}^2} \quad (2)$$

A dimensionless parameter, B , called the biaxiality ratio is defined to normalize the T-stress relative to the effective stress intensity factor (Aliha *et al.* 2013).

$$B = \frac{T\sqrt{\pi a}}{K_{eff}} \quad (3)$$

Similarly, the dimensionless fracture process zone size α is defined to normalize the process zone size r_c relative to the crack length a .

$$\alpha = \sqrt{\frac{2r_c}{a}} \quad (4)$$

2.1 GMTS criterion

The GMTS criterion is a modification of the MTS criterion to account for the effect of the T-stress. According to the GMTS criterion, the crack will initiate along the direction θ_0 where the tangential stress is a maximum and the crack will propagate when the maximum tangential stress attains a critical value $\sigma_{\theta\theta c}$ at a critical distance from the crack tip r_c .

The fracture initiation angle θ_0 can be found by solution of

$$K_I \sin \theta_0 + K_{II} (3 \cos \theta_0 - 1) - \frac{16B\alpha K_{eff}}{3} \cos \theta_0 \sin \left(\frac{\theta_0}{2} \right) = 0 \quad (5)$$

The ratios of K_{If}/K_{Ic} and K_{IIf}/K_{Ic} can be expressed as:

$$\frac{K_{If}}{K_{Ic}} = \frac{1}{\left(\frac{3}{4} \cos \frac{\theta_0}{2} + \frac{1}{4} \cos \frac{3\theta_0}{2} \right) + \frac{K_{IIf}}{K_{If}} \left(-\frac{3}{4} \sin \frac{\theta_0}{2} - \frac{3}{4} \sin \frac{3\theta_0}{2} \right) + \frac{B\alpha K_{eff} \sin^2 \theta_0}{K_{If}}} \quad (6)$$

$$\frac{K_{IIf}}{K_{Ic}} = \frac{1}{\frac{K_{If}}{K_{IIf}} \left(\frac{3}{4} \cos \frac{\theta_0}{2} + \frac{1}{4} \cos \frac{3\theta_0}{2} \right) + \left(-\frac{3}{4} \sin \frac{\theta_0}{2} - \frac{3}{4} \sin \frac{3\theta_0}{2} \right) + \frac{B\alpha K_{eff} \sin^2 \theta_0}{K_{IIf}}} \quad (7)$$

where K_{If} and K_{IIf} are the mode I and mode II stress intensity factors at fracture and K_{Ic} is the stress intensity factor at fracture in a pure mode I test.

2.2 GMTSN criterion

The GMTSN criterion relates fracture initiation to the maximum tangential strain near the crack tip. It assumes

that the crack will initiate when the tangential strain $\varepsilon_{\theta\theta}$ is equal to a critical value ε_T in the direction θ_0 and at a critical distance r_c . The tangential strain $\varepsilon_{\theta\theta}$ can be expressed as

$$\varepsilon_{\theta\theta} = \frac{1+\nu}{4E\sqrt{2\pi r}} \{K_I A_1(\theta) + K_{II} A_2(\theta) + T\sqrt{2\pi r} A_3(\theta)\} \quad (8)$$

where

$$\begin{aligned} A_1(\theta) &= (2k-3)\cos\frac{\theta}{2} + \cos\frac{3\theta}{2} \\ A_2(\theta) &= -(2k-3)\sin\frac{\theta}{2} - 3\sin\frac{3\theta}{2} \\ A_3(\theta) &= (k+1-4\cos^2\theta) \end{aligned} \quad (9)$$

k is an elastic constant, when $k=3-4\nu$ for plane strain problems and $k=(3-\nu)/(1+\nu)$ for plane stress problems.

The initiation crack angle θ_0 can be obtained from

$$K_I \left[(3-2k)\sin\frac{\theta_0}{2} - 3\sin\frac{3\theta_0}{2} \right] + K_{II} \left[(3-2k)\cos\frac{\theta_0}{2} - 9\cos\frac{3\theta_0}{2} \right] + 8B\alpha K_{eff} \sin 2\theta_0 = 0 \quad (10)$$

Finally, the ratios of K_{Iff}/K_{IC} and K_{IIff}/K_{IC} are given by:

$$\frac{K_{Iff}}{K_{IC}} = \frac{2k-2+(B\alpha)_c(k-3)}{A_1(\theta_0) + \frac{K_{IIff}}{K_{Iff}} A_2(\theta_0) + B\alpha \frac{K_{eff}}{K_{Iff}} A_3(\theta_0)} \quad (11)$$

$$\frac{K_{IIff}}{K_{IC}} = \frac{2k-2+(B\alpha)_c(k-3)}{\frac{K_{Iff}}{K_{IIff}} A_1(\theta_0) + A_2(\theta_0) + B\alpha \frac{K_{eff}}{K_{IIff}} A_3(\theta_0)} \quad (12)$$

2.3 GSED criterion

The strain energy density factor S function can be written in a simplified form using the first two terms in Williams infinite expansion as (Ayatollahi *et al.* 2015):

$$S = \frac{1+\nu}{2\pi E} [K_I^2 B_1(\theta) + K_{II}^2 B_2(\theta) + K_I K_{II} B_3(\theta) + \sqrt{2\pi r} K_I T B_4(\theta) + \sqrt{2\pi r} K_{II} T B_5(\theta) + 2\pi r T^2 B_6(\theta)] \quad (13)$$

where

$$\begin{aligned} B_1(\theta) &= \frac{2k-1}{8} + \frac{k-1}{4}\cos\theta - \frac{1}{8}\cos 2\theta \\ B_2(\theta) &= \frac{2k+3}{8} - \frac{k-1}{4}\cos\theta + \frac{3}{8}\cos 2\theta \\ B_3(\theta) &= \frac{1-k}{2}\sin\theta + \frac{1}{2}\sin 2\theta \\ B_4(\theta) &= \frac{2k-3}{4}\cos\frac{\theta}{2} + \frac{1}{4}\cos\frac{5\theta}{2} \\ B_5(\theta) &= -\left(\frac{2k+1}{4}\sin\frac{\theta}{2} + \frac{1}{4}\sin\frac{5\theta}{2}\right) \\ B_6(\theta) &= \frac{k+1}{8} \end{aligned} \quad (14)$$

and k is the same elastic constant defined for the GMTSN criterion.

The crack will initiate in the direction θ_0 where the strain energy density factor S is at a minimum. Fracture is predicted to occur when the strain energy density factor reaches its critical value S_{cr} at a critical distance r_c .

The initiation angle θ_0 is found by solution of

$$K_I^2 C_1(\theta_0) + K_{II}^2 C_2(\theta_0) + K_I K_{II} C_3(\theta_0) + (B\alpha K_{eff}) K_I C_4(\theta_0) + (B\alpha K_{eff}) K_{II} C_5(\theta_0) + (B\alpha K_{eff})^2 C_6(\theta_0) = 0 \quad (15)$$

where

$$\begin{aligned} C_1(\theta_0) &= -\frac{k-1}{4}\sin\theta_0 + \frac{1}{4}\sin 2\theta_0 \\ C_2(\theta_0) &= \frac{k-1}{4}\sin\theta_0 - \frac{3}{4}\sin 2\theta_0 \\ C_3(\theta_0) &= \frac{1-k}{2}\cos\theta_0 + \cos 2\theta_0 \\ C_4(\theta_0) &= -\frac{2k-3}{8}\sin\frac{\theta_0}{2} - \frac{5}{8}\sin\frac{5\theta_0}{2} \\ C_5(\theta_0) &= -\frac{2k+1}{8}\cos\frac{\theta_0}{2} - \frac{5}{8}\cos\frac{5\theta_0}{2} \\ C_6(\theta_0) &= 0 \end{aligned} \quad (16)$$

The ratios of K_{Iff}/K_{IC} and K_{IIff}/K_{IC} can be obtained as:

$$\frac{K_{Iff}}{K_{IC}} = \frac{k-1}{\sqrt{2} \frac{K_{II}^2}{K_{Iff}^2} B_1(\theta_0) + B_2(\theta_0) + \frac{K_{II} K_{Iff}}{K_{Iff}^2} B_3(\theta_0) + \frac{(B\alpha K_{eff})}{K_{Iff}} B_4(\theta_0) + \frac{K_{II} (B\alpha K_{eff})}{K_{Iff} K_{Iff}} B_5(\theta_0) + \left(\frac{B\alpha K_{eff}}{K_{Iff}}\right)^2 B_6(\theta_0)} \quad (17)$$

$$\frac{K_{IIff}}{K_{IC}} = \frac{k-1}{\sqrt{2} \frac{K_{Iff}^2}{K_{II}^2} B_1(\theta_0) + B_2(\theta_0) + \frac{K_{Iff} K_{II}}{K_{II}^2} B_3(\theta_0) + \frac{(B\alpha K_{eff})}{K_{II}} B_4(\theta_0) + \frac{K_{Iff} (B\alpha K_{eff})}{K_{II} K_{II}} B_5(\theta_0) + \left(\frac{B\alpha K_{eff}}{K_{II}}\right)^2 B_6(\theta_0)} \quad (18)$$

3. Experiment and procedures

3.1 Numerical analyses

A schematic representation of three-point bending specimen is shown in Fig. 2. The specimen is a rectangular solid with length L , width W , and thickness B . An edge crack of length a is inclined to the direction of the vertical compressive load (P) with an angle β . We can obtain different combinations of modes I and II fracture by changing the orientation angle β . The stress intensity factors and T-stress are functions of the geometry defined by the relative crack length a/W , the loading span ratio $2S/L$ and the orientation angle β .

$$K_i = \frac{P\sqrt{\pi a}}{2WB} Y_i\left(\frac{a}{W}, \frac{2S}{L}, \beta\right) \quad (19)$$

$$T = \frac{P}{2WB} T^*\left(\frac{a}{W}, \frac{2S}{L}, \beta\right) \quad (20)$$

where i represents mode I and mode II. Y_i and T^* are dimensionless stress intensity factors and dimensionless T-stress.

The commercial finite element software Abaqus 6.14 (Abaqus 6.14 Manual and Versi 2017) was used to calculate the dimensionless Y_i and T^* . The geometry conditions of the model are $L=120$ mm, $W=40$ mm, $B=20$ mm and the orientation angle β is variable. The Young's modulus and Poisson's ratio of sandstone are taken to be $E=20$ GPa, $\nu=0.19$ (Wei *et al.* 2017). The typical mesh pattern for the three-point bending specimen model is shown in Fig. 3. In order to produce the singularity of stress/strain field near the crack tip, CPS6 type singular elements were used in the first ring of elements surrounding the crack tip. All other elements are 8-node CPS8 elements. The loading boundary condition is set as that the left lower support has fixed X and Y displacements while the right side has fixed Y displacement. The vertical load is 80N and the model used plane strain conditions.

Finite element calculations were made for a constant relative crack length $a/W=0.5$ with loading span ratios $2S/L$

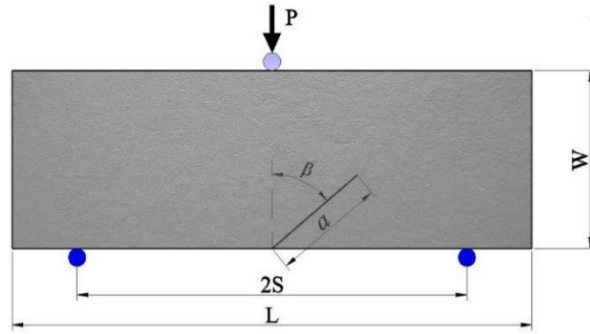


Fig. 2 Geometry diagram of three-point bending specimen

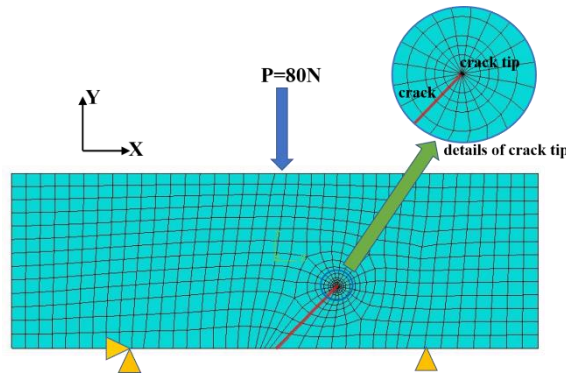


Fig. 3 Finite element model of three-point bending specimen

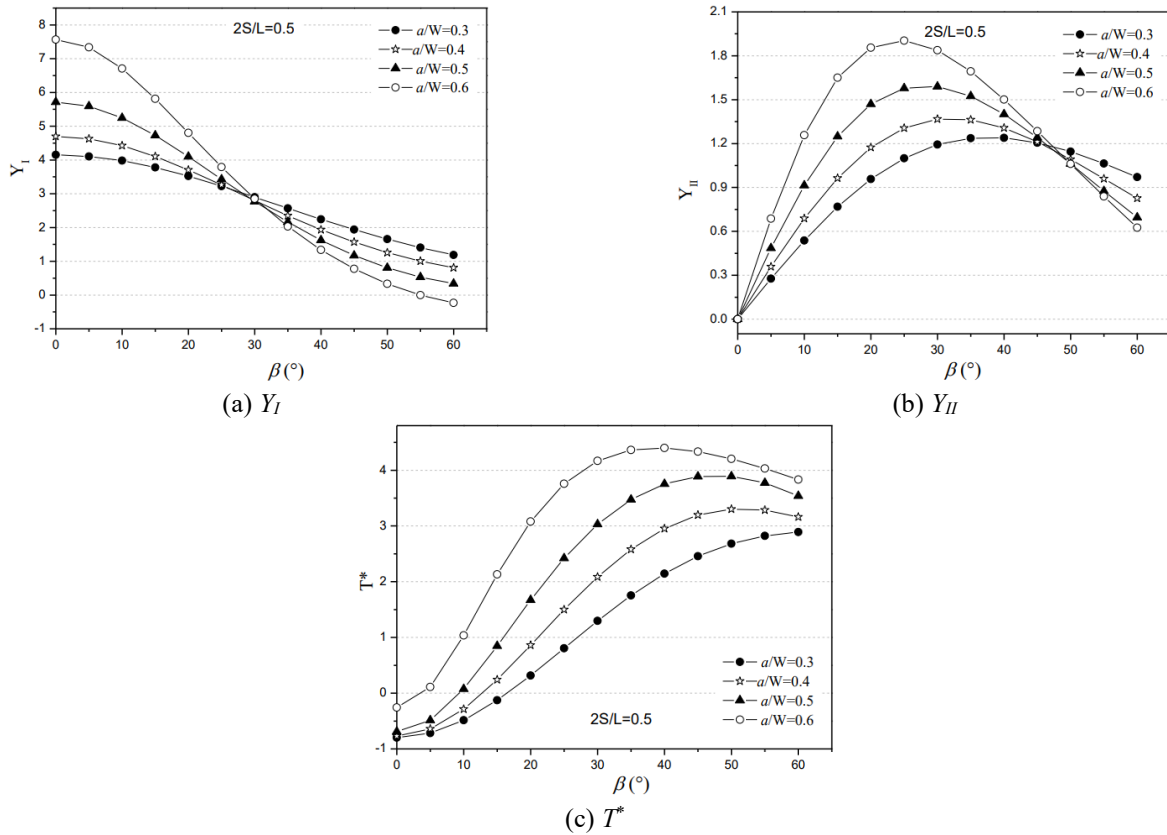


Fig. 4 Dimensionless parameters versus orientation angle for different relative crack lengths: (a) dimensionless parameter Y_I , (b) dimensionless parameter Y_{II} and (c) dimensionless parameter T^*

varying from 0.3 to 0.6 and a constant loading span ratio $2S/L = 0.5$ with relative crack lengths a/W varying from 0.3

to 0.6. The orientation angle β is varies from 0° to 60° . The results are shown in Figs. 4 and 5. It can be seen that

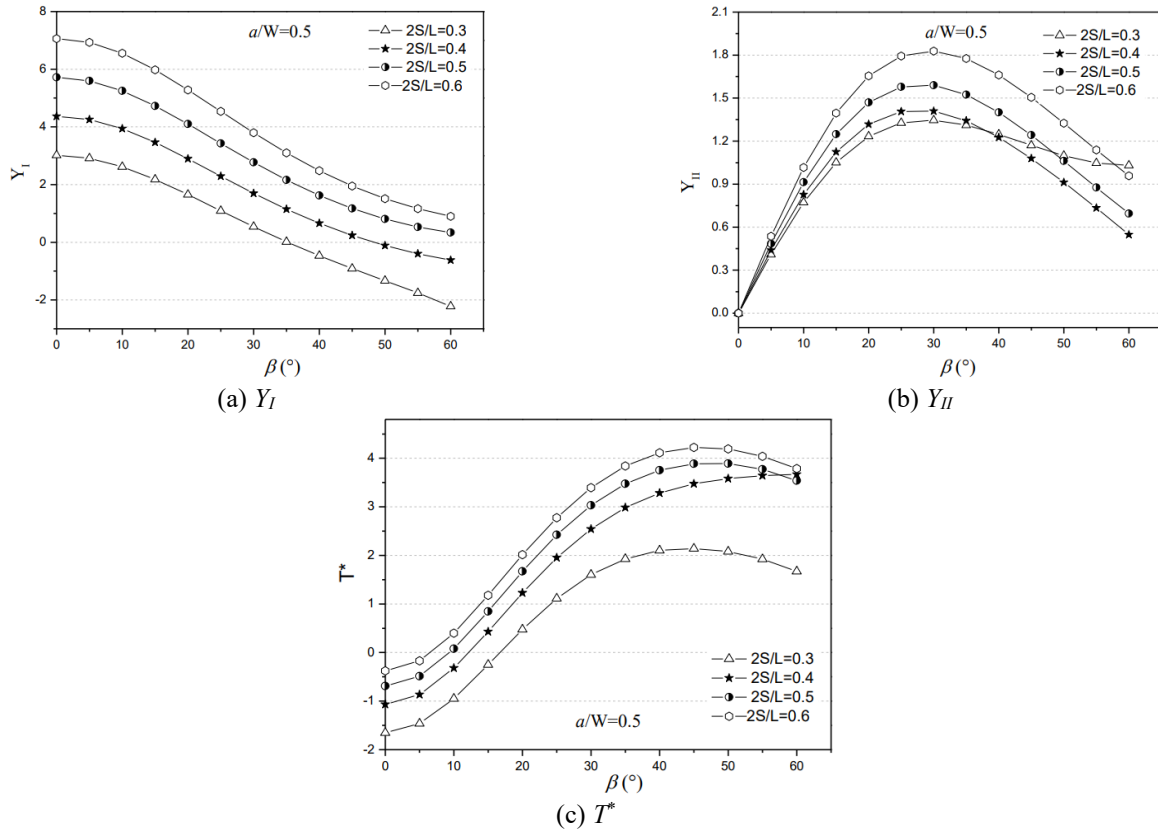


Fig. 5 Dimensionless parameters versus orientation angle for different loading span ratios: (a) dimensionless parameter Y_I , (b) dimensionless parameter Y_{II} and (c) dimensionless parameter T^*

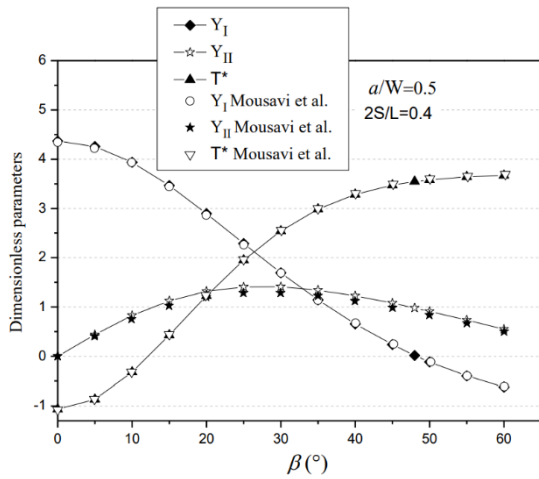


Fig. 6 Dimensionless fracture parameters for test conditions

Table 1 Normalized SIFs and T-stress under test condition

β (°)	Y_I	Y_{II}	T^*
0	4.369	0	-1.067
10	3.939	0.827	-0.321
20	2.894	1.318	1.228
30	1.695	1.409	2.542
40	0.656	1.226	3.284
48	0	0.98	3.546

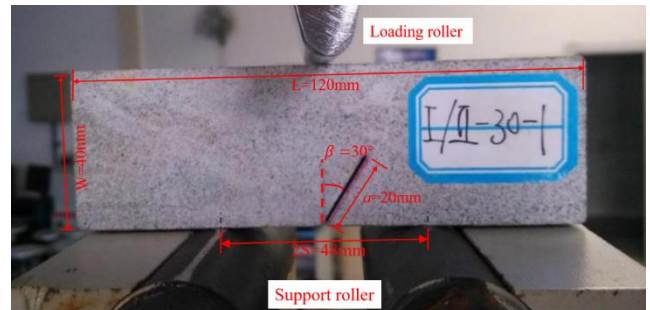


Fig. 7 The experimental setup of three-point bending specimen

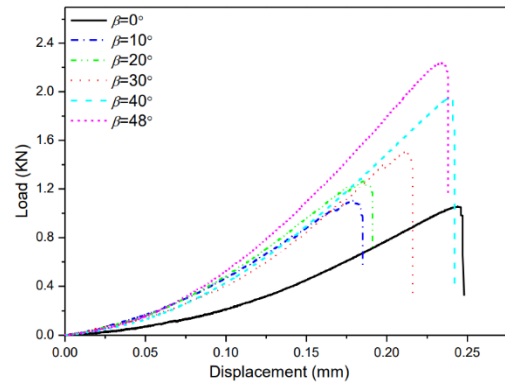


Fig. 8 Typical load-displacement curves for different orientation angles

the dimensionless parameter Y_I decreases as the orientation

angle β increases. Pure mode I exists when $\beta = 0^\circ$. The

Table 2 Experimental results of three-point bending specimen on sandstone (in this table SD means Standard Deviation)

Specimen no.	β (°)	θ_0 (°)	P_{cr} (kN)	P_{cr-avg} (SD)	K_{Ij} (MPa·m ^{0.5})	K_{Ij-avg} (MPa·m ^{0.5})	K_{IIj} (MPa·m ^{0.5})	$K_{IIj-avg}$ (MPa·m ^{0.5})
I/II-0-1	0	0	1.213	1.148 (0.073)	0.830	0.786	0	0
I/II-0-2	0	0	1.225		0.838		0	
I/II-0-3	0	0	1.099		0.752		0	
I/II-0-4	0	0	1.055		0.722		0	
I/II-10-1	10	-21	1.107	1.197 (0.088)	0.683	0.739	0.143	0.155
I/II-10-2	10	-17	1.298		0.801		0.168	
I/II-10-3	10	-24	1.272		0.785		0.165	
I/II-10-4	10	-23	1.112		0.686		0.144	
I/II-20-1	20	-42	1.236	1.291 (0.049)	0.560	0.585	0.255	0.266
I/II-20-2	20	-44	1.295		0.587		0.267	
I/II-20-3	20	-48	1.367		0.620		0.282	
I/II-20-4	20	-45	1.264		0.573		0.261	
I/II-30-1	30	-59	1.489	1.582 (0.083)	0.395	0.420	0.329	0.349
I/II-30-2	30	-63	1.692		0.449		0.373	
I/II-30-3	30	-61	1.517		0.403		0.335	
I/II-30-4	30	-67	1.631		0.433		0.360	
I/II-40-1	40	-78	1.837	1.820 (0.088)	0.189	0.187	0.353	0.350
I/II-40-2	40	-76	1.793		0.184		0.344	
I/II-40-3	40	-71	1.703		0.175		0.327	
I/II-40-4	40	-77	1.948		0.200		0.374	
I/II-48-1	48	-80	2.234	2.240 (0.187)	0	0	0.343	0.344
I/II-48-2	48	-85	2.544		0		0.391	
I/II-48-3	48	-84	2.128		0		0.327	
I/II-48-4	48	-82	2.054		0		0.315	

dimensionless parameters Y_{II} and T^* first increase then decrease as the orientation angle β increases

Pure mode II occurs when the mode I stress intensity factor $K_I=0$ and the mode II stress intensity factor $K_{II}\neq 0$ (Ayatollahi and Zakeri 2017, Ayatollahi and Aliha 2005). From Figs. 4(a) and 5(a), it can be observed that the dimensionless parameter Y_I becomes equal to 0 when the inclined angle β is large enough, so this type of specimen can be used to conduct a series of fracture tests for the complete range of mode mixities. When the span length ratio is constant, the larger the relative crack length the lower the orientation angle for pure mode II. Also, when the relative crack length is fixed, the smaller the span length ratio is, the smaller the orientation angle needs to be to achieve pure mode II. Large orientation angles are difficult to achieve in practice without damaging the specimens, therefore large relative crack lengths and small span to length ratios need to be chosen.

3.2 Fracture tests and results

The sandstone used in the experiments was a green sandstone from Sichuan province, China and has a fine grain with good uniformity. Specimens were cut from a large block using a circular saw with the dimensions

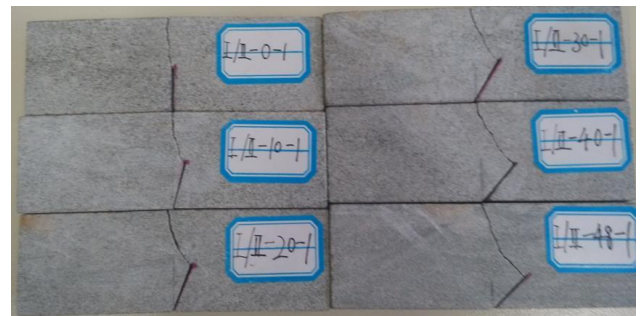


Fig. 9 Representative photographs of specimens taken after test for the complete range of crack orientation angles

$L=120$ mm, $W=40$ mm and $B=20$ mm. A relative crack length of $a/W=0.5$ ($a=20$ mm) was used and the span to length ratio was $2S/L=0.4$. To produce the cracks in the specimens, a notch with a width of 1mm and nearly 19 mm in length was introduced using a circular saw. Finally, the crack tip was sharpened by a diamond wire saw with a diameter of 0.26 mm to obtain the desired crack length of $a=20$ mm. Note that the International Society for Rock Mechanics and Rock Engineering (ISRM) suggested method for pure mode I testing is to use a cracked chevron notched Brazilian disc (CCNBD) specimen with a crack

width less than 1.5 mm (Fowell *et al.* 1995).

The dimensionless parameters Y_I , Y_{II} and T^* corresponding to the experimental conditions calculated by FEM and literature (Mousavi *et al.* 2019) are shown in Fig. 6. The dimensionless values calculated in this paper are consistent with those in the literature. It can be seen that when the crack orientation angle is given approximately by $\beta=48.4^\circ$, Y_I is equal to 0 and pure mode II conditions arise. Therefore, the orientation angles used in the tests were set to $\beta=\{0^\circ, 10^\circ, 20^\circ, 30^\circ, 40^\circ, 48^\circ\}$ to investigate mode mixities from pure mode I to pure mode II. For each orientation angle, 4 identical specimens were used to assess the scatter of the results.

An RGM-4300 universal servo-hydraulic tension and compression test machine was used to conduct this fracture test, using displacement-controlled mode with a constant loading rate of 0.05 mm/min to ensure quasi-static loading. Except for the initial part of the loading, the load-displacement curves for all the tests were nearly straight lines, and the sandstone fractured immediately once the load reached a critical value. The experimental setup and the typical load-displacement curves for the experiment under different orientation angles are shown in Figs. 7 and 8. It can be seen that the fracture load increases with increasing orientation angle and as the proportion of mode II increases.

Substituting the critical load P_{cr} we obtained from fracture tests into Eq. (19), stress intensity factors at fracture can be calculated, as shown in Table 2. When the orientation angles are 0° and 48° , the mean stress intensity factors at fracture for pure mode I and II are calculated to be $0.786 \text{ MPa}\cdot\text{m}^{0.5}$ and $0.344 \text{ MPa}\cdot\text{m}^{0.5}$. These values compare with measurements obtained by other researchers of $0.67\sim 2.56 \text{ MPa}\cdot\text{m}^{0.5}$ for sandstone in pure mode I and $0.32\sim 0.41 \text{ MPa}\cdot\text{m}^{0.5}$ in pure mode II (Guo *et al.* 1993, Ouchterlony 1988, Ouchterlony 1990, Singh 1989).

Photographs of the specimens taken after fracture for different mode mixities fracture are shown in Fig. 9. It is shown that the crack propagated along the initial crack only under pure mode I conditions, and that I/II mixed mode crack paths deviate from the direction of the initial crack. Most of the cracks initiated from the crack tips, only a small number of cracks initiated near the crack tips when the orientation angle is large. This phenomenon has also been observed in experiments by Aliha *et al.* (2010). Their occurrence is considered to be due to small flaws introduced during the manufacturing procedure.

In order to obtain the fracture initiation angles, a tangent line was drawn from the crack tip along the direction of crack initiation. Positive fracture initiation angles are measured clockwise from the crack tip shown in Figure 2 in literature by Aliha *et al.* (2013). Then, the direction of crack propagation relative to the original crack orientation was measured manually from the photographs and depended of the level of mode mixity.

4. Comparison and discussion

The fracture criteria described in Section 2 can be used to provide predictions for the variation of the initiation

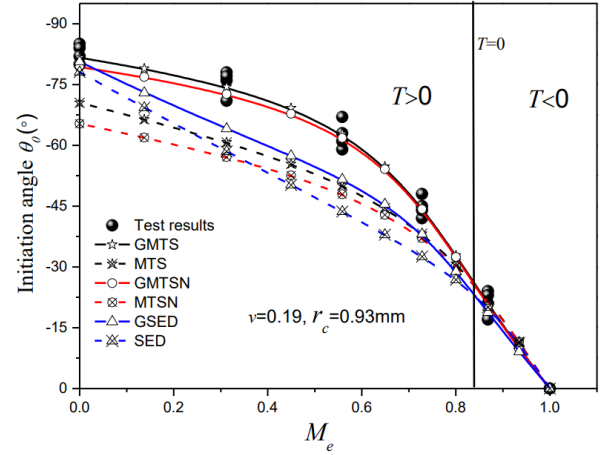


Fig. 10 Comparison between predicting results of different criteria and test data

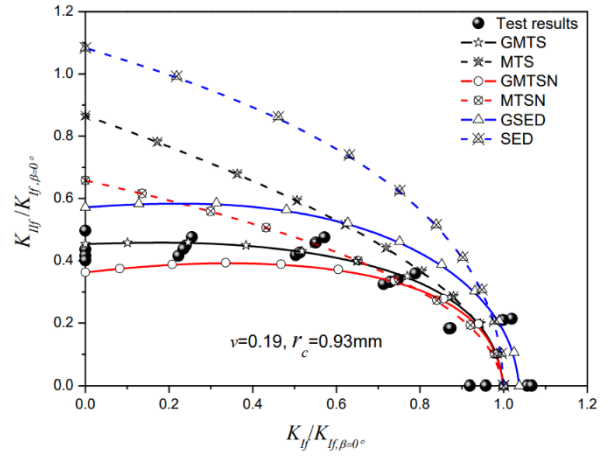


Fig. 11 Predictions of mixed mode fracture loci for different criteria

angle θ_0 with mode mixity for comparison with the experimental results presented in Table 2.

To allow these comparisons to be made, a representative value for the critical distance r_c must be derived. In this work the calculation proposed by Schmidt has been used (Schmidt 1980, Akbardoost and Ayatollahi 2014).

$$r_c = \frac{1}{2\pi} \left(\frac{K_{Ic}}{\sigma_T} \right)^2 \quad (21)$$

where σ_T is the tensile strength of the material, and K_{Ic} is the pure mode I fracture toughness.

Using the mean mode I fracture toughness of sandstone of $0.786 \text{ MPa}\cdot\text{m}^{0.5}$, and the tensile strength of sandstone $\sigma_T = 10.3 \text{ MPa}$ for the mixed mode fracture is then from (Li *et al.* 2018). The critical distance r_c is calculated by Eq. (21) to be 0.93 mm.

A parameter M_e is defined to describe the mode mixity

$$M_e = \frac{2}{\pi} \arctan\left(\frac{K_I}{K_{II}}\right) \quad (22)$$

The value of M_e ranges from 0 to 1. $M_e = 1$ corresponds to pure mode I and $M_e = 0$ to pure mode II.

The plane strain condition was used to predict the fracture properties since the thickness of specimen is

Table 3 Experimental results for additional mode I tests

Specimen no.	β (°)	θ_0 (°)	P_{cr} (N)	P_{cr-avg} (SD)	K_{Ij} (MPa·m ^{0.5})	K_{Ij-avg} (MPa·m ^{0.5})	T (MPa)	T_{avg} (MPa)
Add-1	0	0	451.496		0.673		0.0183	
Add-2	0	0	474.716	453.051	0.707	0.681	0.0193	0.0186
Add-3	0	0	459.236	(12.211)	0.684		0.0186	
Add-4	0	0	443.756		0.661		0.0180	

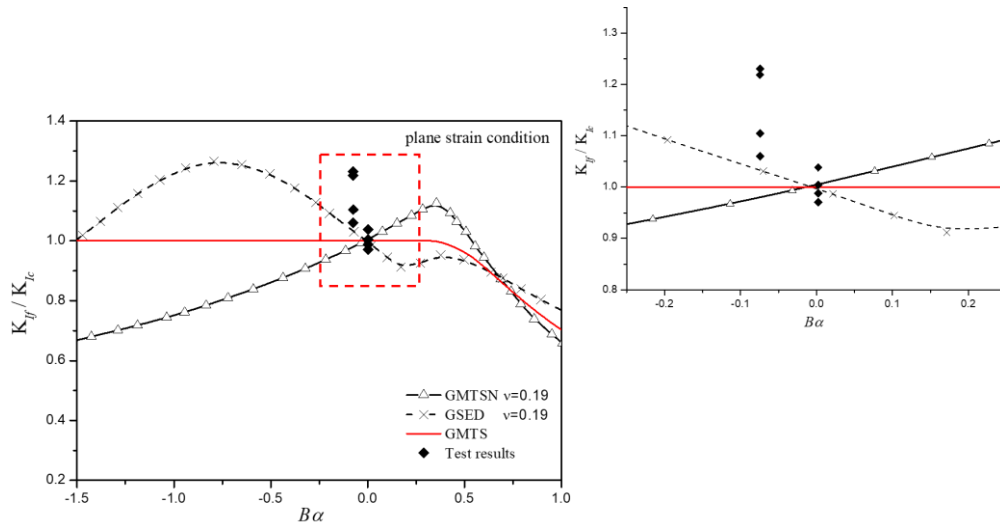


Fig. 12 Effects of T-stress on apparent fracture toughness predicted by different criteria

comparable to the in-plane dimensions. Poisson's ratio for sandstone is taken as $\nu=0.19$ (Wei *et al.* 2017). Fig. 10 shows the results of the comparison of initiation angle with mode mixity using the modified GMTS, GMTSN and GSED criteria. Fig. 10 also shows the results of the conventional MTS, MTSN and SED criteria. These results are calculated from the GMTS, GMTSN and GSED criteria by setting the T-stress equal to zero. The modified criteria generally achieve a better comparison with the experimental results than the conventional criteria. The GMTS and GMTSN criteria show better agreement than the GSED criterion.

Next the fracture criteria will be used to predict the variation of the stress intensity factors at fracture with mode mixity, allowing a comparison of these predictions with the experimental results. The results are shown in Fig 11. In Fig.11, the critical stress intensity factors at fracture of mixed mode I+II have been normalised using the critical SIF at fracture in pure mode I ($K_{Ij, \beta=0^\circ}$). Again, the modified criteria show better comparison with experiment than the conventional criteria. The GMTS criterion provides the best agreement.

Semi-circular (SCB) and edge cracked triangular (ECT) specimens are two other types of specimen containing an inclined edge crack and subjected to three-point bend loading. Both these specimens have simple geometry and need only simple loading configurations. Mousavi *et al.* (2019) have concluded that the state of mode-mixity of the specimen used in this research is not markedly sensitive to the change of crack angle, which is an advantage compared with other geometries of bend specimens.

Recent studies also shown that the T-stress may have an influence on pure mode I fracture (Ayatollahi and Sedighiani 2012, Wei *et al.* 2017, Ayatollahi *et al.* 2002). It has been found also that the crack may not propagate in a self-similar manner in mode I loading when a large positive T-stress exists (Ayatollahi *et al.* 2016, Chao *et al.* 2001). This phenomenon is also observed in the predictions of different generalized criteria (Ayatollahi and Sedighiani 2012, Wei *et al.* 2017, Ayatollahi *et al.* 2002).

To examine the effect of T-stress on pure mode I fracture, an additional set of tests were carried out using a three-point bending specimen with the same dimensions and crack length as the previous tests but a different loading span ratio of $2S/L=0.75$. For these specimens, the T-stress was positive. The test results are shown in Table 3.

For these specimens the nondimensional parameter Ba is equal to 2.20×10^{-3} while for the previous pure mode I specimen with a loading span ratio of $2S/L=0.4$, Ba is equal to -7.45×10^{-2} . For these additional tests, the small value of T-stress was taken to be close to zero and therefore the average value for the stress intensity factor at failure was taken to be the critical stress intensity factor $K_{Ic} = 0.683 \text{ MPa m}^{0.5}$.

For all pure mode I specimens tested, the fracture initiation angles listed in Tables 2 and 3 were all approximately equal to zero. The initiation angle for mode I fracture predicted by the GMTS criterion is provided by Eq. (5) and is equal to zero when $Ba < 0.375$ (Ayatollahi *et al.* 2002). Similarly, Eq. (10) gives the initiation angle for the GMTSN criterion and is equal to zero for $Ba < (3 + k)/16$. Finally, for the GSED criterion, Eq. (15) predicts an

initiation angle of zero for $B\alpha < (6 - 2k)/(k + 11)$. Substituting the Poisson's ratio of sandstone into these condition for a zero initiation angle gives 0.375, 0.3275, and 0.1148 for the GMTS, GMTSN and GSED criteria. These values are all larger than those achieved in the tests.

Fig. 12 shows the normalized stress intensity factor at fracture versus $B\alpha$ predicted for the three modified criteria, for pure mode I fracture calculated using Eq. (6), (11) and (17). The figure also shows the individual tests results corresponding to the two values of $B\alpha$ equal to -7.45×10^{-2} and 2.20×10^{-3} . The test results show a marked increase in nominal stress intensity factor at fracture as $B\alpha$ reduces. In comparison the GMTS criterion predicts no change in stress intensity factor at failure for the range of values of $B\alpha$ covered by the test results while the GMTSN predicts a reduction as $B\alpha$ reduces. The GSED criteria is the only criteria that gives predictions matching the trend of the test results.

5. Conclusions

Mixed mode fracture tests have been conducted using three-point bending specimens, covering the complete range from pure mode I to pure mode II. The critical fracture load increased with orientation angle and with the proportion of mode II loading. The fracture toughness of green sandstone measured in this research was $0.786 \text{ MPa}\cdot\text{m}^{0.5}$ for pure mode I loading and $0.344 \text{ MPa}\cdot\text{m}^{0.5}$ for pure mode II respectively. These values are comparable with other measurements reported in the literature.

For three-point bending specimens under mixed-mode loading the T-stress is generally positive which acts to decrease the effective fracture toughness of the material. The results of the fracture tests have been compared with predictions of conventional and modified mixed mode criteria, where modified criteria include the influence of T-stress. The modified GMTS criterion shows the best agreement with the test results. Pure mode I tests were carried out for two geometries of specimen providing approximately zero and negative T-stress. For these tests, the GSED criterion gave the best agreement.

References

- Akbardoost, J. and Ayatollahi, M.R. (2014), "Experimental analysis of mixed mode crack propagation in brittle rocks: The effect of non-singular terms", *Eng. Fract. Mech.*, **129**, 77-89. <http://doi.org/10.1016/j.engfracmech.2014.05.016>.
- Aliha, M.R.M. and Ayatollahi, M.R. (2011), "Mixed mode I/II brittle fracture evaluation of marble using SCB specimen", *Procedia Eng.*, **10**, 311-318. <http://doi.org/10.1016/j.proeng.2011.04.054>.
- Aliha, M.R.M. and Bahmani, A. (2017), "Rock fracture toughness study under mixed mode I/III loading", *Rock Mech. Rock Eng.*, **50**(7), 1739-1751. <https://doi.org/10.1007/s00603-017-1201-7>.
- Aliha, M.R.M., Ayatollahi, M.R., Smith, D.J. and Pavier, M.J. (2010), "Geometry and size effects on fracture trajectory in a limestone rock under mixed mode loading", *Eng. Fract. Mech.*, **77**(11), 2200-2212. <http://doi.org/10.1016/j.engfracmech.2010.03.009>.
- Aliha, M.R.M., Bagherifard, S., Akhondi, Sh., Mousavi, S.S., Mousavi, A. and Parsania, H. (2018), "Fracture and microstructural study of bovine bone under mixed mode I/II loading", *Procedia Struct. Integrit.*, **13**, 1488-1493. <http://doi.org/10.1016/j.prostr.2018.12.306>.
- Aliha, M.R.M., Bahmani, A. and Akhondi, S. (2015a), "Numerical analysis of a new mixed mode I/III fracture test specimen", *Eng. Fract. Mech.*, **134**, 95-110. <https://doi.org/10.1016/j.engfracmech.2014.12.010>.
- Aliha, M.R.M., Bahmani, A. and Akhondi, S. (2015b), "Determination of mode III fracture toughness for different materials using a new designed test configuration", *Mater. Des.*, **86**, 863-871. <https://doi.org/10.1016/j.matdes.2015.08.033>.
- Aliha, M.R.M., Hosseinpour, G.R. and Ayatollahi, M.R. (2013), "Application of cracked triangular specimen subjected to three-point bending for investigating fracture behavior of rock materials", *Rock Mech. Rock Eng.*, **46**(5), 1023-1034. <http://doi.org/10.1007/s00603-012-0325-z>.
- Aliha, M.R.M., Shaker, S. and Keymanesh, M.R. (2019), "Low temperature fracture toughness study for bitumen under mixed mode I+ II loading condition", *Eng. Fract. Mech.*, **206**, 297-309. <http://doi.org/10.1016/j.engfracmech.2018.11.037>.
- Aliha, M.R.M., Sistaninia, M., Smith, D.J., Pavier, M.J. and Ayatollahi, M.R. (2012), "Geometry effects and statistical analysis of mode I fracture in giting limestone", *Int. J. Rock Mech. Min. Sci.*, **51**, 128-135. <https://doi.org/10.1016/j.ijrmms.2012.01.017>.
- Ayatollahi, M.R. and Akbardoost, J. (2012), "Size effects on fracture toughness of quasi-brittle materials—A new approach", *Eng. Fract. Mech.*, **92**, 89-100. <https://doi.org/10.1016/j.engfracmech.2012.06.005>.
- Ayatollahi, M.R. and Akbardoost, J. (2013), "Size effects in mode II brittle fracture of rocks", *Eng. Fract. Mech.*, **112**, 165-180. <https://doi.org/10.1016/j.engfracmech.2013.10.011>.
- Ayatollahi, M.R. and Aliha, M.R.M. (2005), "Cracked Brazilian disc specimen subjected to mode II deformation", *Eng. Fract. Mech.*, **72**(4), 493-503. <http://dx.doi.org/10.1016/j.engfracmech.2004.05.002>.
- Ayatollahi, M.R. and Aliha, M.R.M. (2008), "On the use of Brazilian disc specimen for calculating mixed mode I-II fracture toughness of rock materials", *Eng. Fract. Mech.*, **75**(16), 4631-4641. <http://doi.org/10.1016/j.engfracmech.2008.06.018>.
- Ayatollahi, M.R. and Sedighiani, K. (2012), "Mode I fracture initiation in limestone by strain energy density criterion", *Theor. Appl. Fract. Mech.*, **57**(1), 14-18. <http://doi.org/10.1016/j.tafmec.2011.12.003>.
- Ayatollahi, M.R. and Sistaninia, M. (2011), "Mode II fracture study of rocks using Brazilian disk specimens", *Int. J. Rock Mech. Min. Sci.*, **48**(5), 819-826. <https://doi.org/10.1016/j.ijrmms.2011.04.017>.
- Ayatollahi, M.R. and Zakeri, M. (2017), "An improved definition for mode I and mode II crack problems", *Eng. Fract. Mech.*, **175**, 235-246. <http://doi.org/10.1016/j.engfracmech.2017.01.027>.
- Ayatollahi, M.R., Berto, F., Campagnolo, A., Gallo, P. and Tang, K. (2017), "Review of local strain energy density theory for the fracture assessment of V-notches under mixed mode loading", *Eng. Solid Mech.*, **5**(2), 113-132. <http://doi.org/10.5267/j.esm.2017.3.001>.
- Ayatollahi, M.R., Moghaddam, M.R. and Berto, F. (2015), "A generalized strain energy density criterion for mixed mode fracture analysis in brittle and quasi-brittle materials", *Theor. Appl. Fract. Mech.*, **79**, 70-76. <http://doi.org/10.1016/j.tafmec.2015.09.004>.
- Ayatollahi, M.R., Moghaddam, M.R., Razavi, S.M.J. and Berto, F. (2016), "Geometry effects on fracture trajectory of PMMA

- samples under pure mode-I loading”, *Eng. Fract. Mech.*, **163**, 449-461. <http://doi.org/10.1016/j.engfracmech.2016.05.014>.
- Ayatollahi, M.R., Pavier, M.J. and Smith, D.J. (2002), “Mode I cracks subjected to large T-stresses”, *Int. J. Fract.*, **117**(2), 159-174. <https://doi.org/10.1023/A:1020973802643>.
- Campagnolo, A. and Berto, F. (2017), “Some recent criteria for brittle fracture assessment under mode II loading”, *Eng. Solid Mech.*, **5**(1), 31-38. <http://doi.org/10.5267/j.esm.2016.10.002>.
- Chang, K.J. (1981), “On the maximum strain criterion—a new approach to the angled crack problem”, *Eng. Fract. Mech.*, **14**(1), 107-124. [https://doi.org/10.1016/0013-7944\(81\)90021-7](https://doi.org/10.1016/0013-7944(81)90021-7).
- Chao, Y.J., Liu, S. and Broviak, B.J. (2001), “Brittle fracture: variation of fracture toughness with constraint and crack curving under mode I conditions”, *Exp. Mech.*, **41**(3), 232-241. <http://doi.org/10.1007/BF02323139>.
- Erdogan, F. and Sih, G.C. (1963), “On the crack extension in plates under plane loading and transverse shear”, *J. Basic Eng.*, **85**(4), 519-525. <http://dx.doi.org/10.1115/1.3656897>.
- Fowell, R.J., Hudson, J.A., Xu, C., Chen, J. and Zhao, X. (1995), “Suggested method for determining mode I fracture toughness using cracked chevron notched Brazilian disc (CCNBD) specimens”, *Int. J. Rock Mech. Min. Sci. Geomech. Abstr.*, **7**(32), 57-64. [http://dx.doi.org/10.1016/0148-9062\(94\)00015-U](http://dx.doi.org/10.1016/0148-9062(94)00015-U).
- Guo, H., Aziz, N.I. and Schmidt, L.C. (1993), “Rock fracture-toughness determination by the Brazilian test”, *Eng. Geol.*, **33**(3), 177-188. [http://doi.org/10.1016/0013-7952\(93\)90056-I](http://doi.org/10.1016/0013-7952(93)90056-I).
- Hibbitt, Karlsson & Sorensen, Inc. (2017), *Abaqus 6.14 Manual*, Version 6.14, Hibbitt, Karlsson & Sorensen, Inc.
- Hua, W., Dong, S., Pan, X. and Wang, Q. (2017), “Mixed mode fracture analysis of CCBD specimens based on the extended maximum tangential strain criterion”, *Fatigue Fract. Eng. Mater. Struct.*, **40**(12), 2118-2127. <http://doi.org/10.1111/ffe.12638>.
- Kumar, C.N.S., Krishna, P. and Kumar, D.R. (2017), “Effect of fiber and aggregate size on mode-I fracture parameters of high strength concrete”, *Adv. Concrete Constr.*, **5**(6), 613-624. <https://doi.org/10.12989/acc.2017.5.6.613>.
- Li, Y., Dong, S., Li, K. and Hua, W. (2018), “Numerical simulation and experimental study of three-point bending specimen’s I/II mixed mode fracture”, *J. Exp. Mech.*, **33**(4), 557-566. <https://doi.org/10.7520/1001-4888-17-040>.
- Maruvanchery, V. and Kim, E. (2019), “Effects of water on rock fracture properties: Studies of mode I fracture toughness, crack propagation velocity, and consumed energy in calcite-cemented sandstone”, *Geomech. Eng.*, **17**(1), 57-67. <https://doi.org/10.12989/gae.2019.17.1.057>.
- Midhun, M.S., Rao, T.D.G. and Srikrishna, T.C. (2018), “Mechanical and fracture properties of glass fiber reinforced geopolymer concrete”, *Adv. Concrete Constr.*, **6**(1), 29-45. <https://doi.org/10.12989/acc.2018.6.1.029>.
- Mirsayar, M.M. (2015), “Mixed mode fracture analysis using extended maximum tangential strain criterion”, *Mater. Des.*, **86**, 941-947. <http://doi.org/10.1016/j.matdes.2015.07.135>.
- Mirsayar, M.M., Berto, F., Aliha, M.R.M. and Park, P. (2016), “Strain-based criteria for mixed-mode fracture of polycrystalline graphite”, *Eng. Fract. Mech.*, **156**, 114-123. <https://doi.org/10.1016/j.engfracmech.2016.02.011>.
- Mirsayar, M.M., Razmi, A., Aliha, M.R.M. and Berto, F. (2018), “EMTSN criterion for evaluating mixed mode I/II crack propagation in rock materials”, *Eng. Fract. Mech.*, **190**, 186-197. <https://doi.org/10.1016/j.engfracmech.2017.12.014>.
- Mousavi, S.S., Aliha, M.R.M. and Imani, D.M. (2020), “On the use of edge cracked short bend beam specimen for PMMA fracture toughness testing under mixed-mode I/II”, *Polym. Test.*, **81**, 106199. <https://doi.org/10.1016/j.polymertesting.2019.106199>.
- Ouchterlony, F. (1988), “Suggested methods for determining the fracture toughness of rock”, *Int. J. Rock Mech. Min. Sci. Geomech. Abstr.*, **25**, 71-96.
- Ouchterlony, F. (1990), “Fracture toughness testing of rock with core based specimens”, *Eng. Fract. Mech.*, **35**(1-3), 351-366. [http://doi.org/10.1016/0013-7944\(90\)90214-2](http://doi.org/10.1016/0013-7944(90)90214-2).
- Pour, P.J.H., Aliha, M.R.M. and Keymanesh, M.R. (2018), “Evaluating mode I fracture resistance in asphalt mixtures using edge notched disc bend ENDB specimen with different geometrical and environmental conditions”, *Eng. Fract. Mech.*, **190**, 245-258. <https://doi.org/10.1016/j.engfracmech.2017.11.007>.
- Razavi, S.M.J., Aliha, M.R.M. and Berto, F. (2018), “Application of an average strain energy density criterion to obtain the mixed mode fracture load of granite rock tested with the cracked asymmetric four-point bend specimens”, *Theor. Appl. Fract. Mech.*, **97**, 419-425. <https://doi.org/10.1016/j.tafmec.2017.07.004>.
- Richard, H.A. and Benitz, K. (1983), “A loading device for the creation of mixed mode in fracture mechanics”, *Int. J. Fract.*, **22**(2), R55-R58. <http://dx.doi.org/10.1007/BF00942726>.
- Rizov, V. (2013), “Mixed-mode I/II fracture study of polymer composites using Single Edge Notched Bend specimens”, *Comput. Mater. Sci.*, **77**, 1-6. <http://doi.org/10.1016/j.commatsci.2013.04.021>.
- Schmidt, R.A. (1980), “A microcrack model and its significance to hydraulic fracturing and fracture toughness testing”, *Proceedings of 21st US symposium on Rock Mechanics*, Rolla, Missouri, U.S.A., May.
- Shaker, S., Aliha, M.M. and Keymanesh, M. (2019), “Aging effect on combined mode fracture resistance of bitumen”, *Fatigue Fract. Eng. Mater. Struct.*, **42**(7), 1609-1621. <https://doi.org/10.1111/ffe.13003>.
- Sih, G.C. (1973), “Some basic problems in fracture mechanics and new concepts”, *Eng. Fract. Mech.*, **5**(2), 365-377. [http://doi.org/10.1016/0013-7944\(73\)90027-1](http://doi.org/10.1016/0013-7944(73)90027-1).
- Sih, G.C. (1974), “Strain-energy-density factor applied to mixed mode crack problems”, *Int. J. Fract.*, **10**(3), 305-321. <http://dx.doi.org/10.1007/BF00035493>.
- Singh, R.N. and Sun, G.X. (1989), *Relationships Between Fracture Toughness, Hardness Indices and Mechanical Properties of Rocks*, Mining Department Magazine, XLI, 49-62.
- Smith, D.J., Ayatollahi, M.R. and Pavier, M.J. (2001), “The role of T-stress in brittle fracture for linear elastic materials under mixed-mode loading”, *Fatigue Fract. Eng. Mater. Struct.*, **24**(2), 137-150. <http://doi.org/10.1046/j.1460-2695.2001.00377.x>.
- Wei, M.D., Dai, F., Xu, N.W., Liu, Y. and Zhao, T. (2017), “Fracture prediction of rocks under mode I and mode II loading using the generalized maximum tangential strain criterion”, *Eng. Fract. Mech.*, **186**, 21-38. <http://doi.org/10.1016/j.engfracmech.2017.09.026>.
- Williams, M.L. (1957), “On the stress distribution at the base of a stationary crack”, *J. Appl. Mech.*, **24**, 109-114. <https://doi.org/10.1115/1.3640470>.
- Yukio, U., Kazuo, I., Tetsuya, Y. and Mitsuru, A. (1983), “Characteristics of brittle fracture under general combined modes including those under bi-axial tensile loads”, *Eng. Fract. Mech.*, **18**(6), 1131-1158. [http://doi.org/10.1016/0013-7944\(83\)90007-3](http://doi.org/10.1016/0013-7944(83)90007-3).